

Supplementary Information

Electrochemical production of H₂O₂ on palladium-based clusters driven by metal-support interaction

Prabhu Bharathan,^a Can Li,^b Bo Zhao,^c Anna Dennett,^a Lihua Zhang^{*,d} and Jiye Fang^{*,a,b}

^aMaterials Science and Engineering Program, State University of New York at Binghamton, Binghamton, New York 13902, United States.

^bDepartment of Chemistry, State University of New York at Binghamton, Binghamton, New York 13902, United States.

^cCollege of Arts & Sciences Microscopy, Texas Tech University, Lubbock, Texas 79409, United States.

^dCenter for Functional Nanomaterials, Brookhaven National Laboratory, Upton, New York 11973, United States.

Contents

1. Supplementary Figures
2. Supplementary Tables
3. References

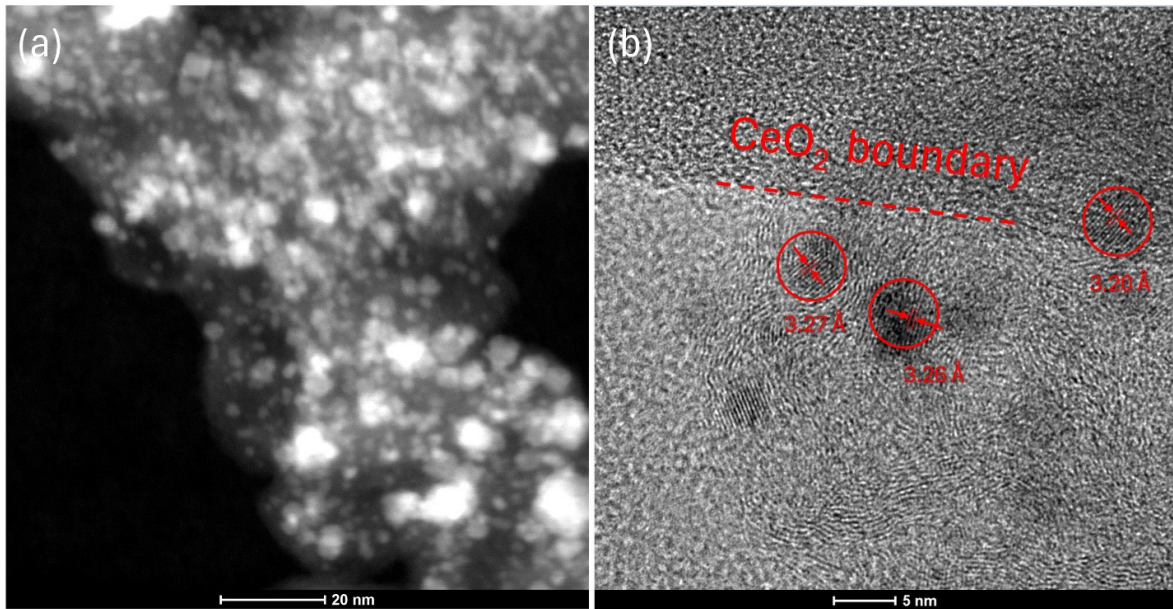


Figure S1. Electron microscopic images of the Pd_{1.53}-CeO₂/C sample. (a), HAADF-STEM image, showing the low-magnification Pd-component and CeO₂ nanocrystal distribution on the carbon support; (b), HRTEM image, where red circles highlight PdO NCs with the measured *d*-spacings of their lattice planes.

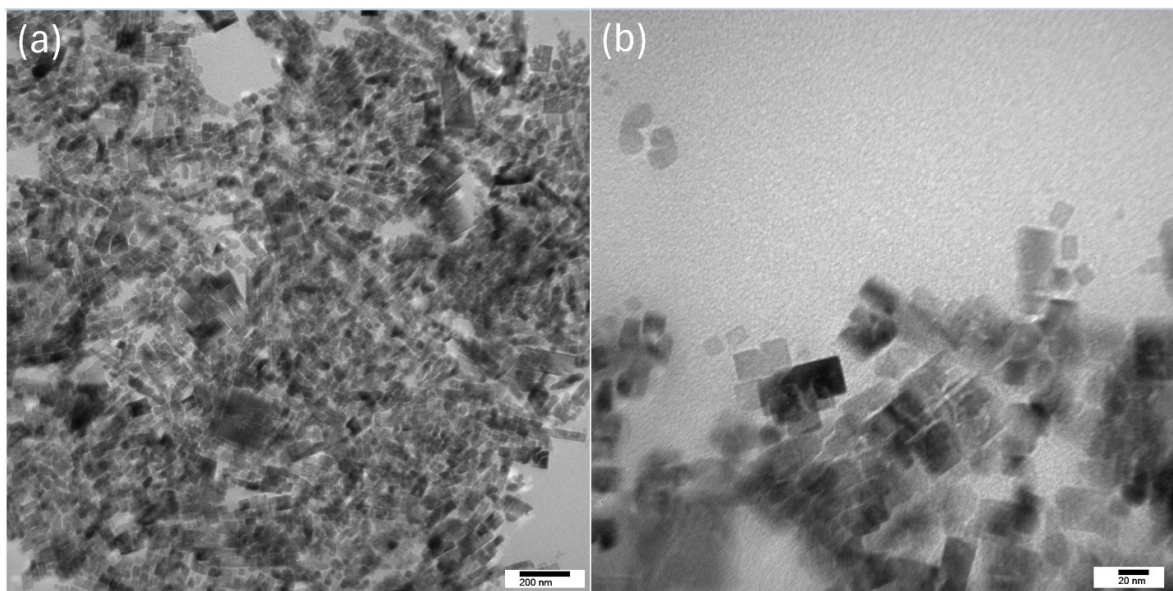


Figure S2. TEM images of individual CeO₂ substrates without Pd element and carbon, synthesized using the same procedure.

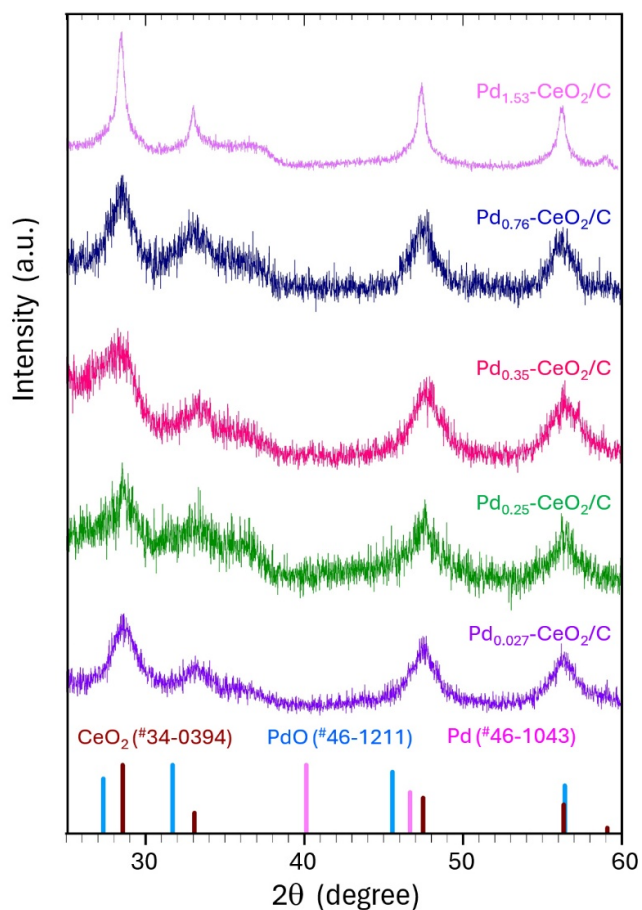


Figure S3. XRD patterns of Pd_x-CeO₂/C composites ($x = 0.027, 0.25, 0.35, 0.76, 1.53$). The vertical lines indicate the standard diffraction pattern of CeO₂ (ICDD PDF card 34-0394), PdO (ICDD PDF card 46-1211), and Pd (ICDD PDF card 46-1043).

Table S1. Pd Loadings of the input set and actual loadings determined by ICP-OES analysis

Set Pd loading (wt %) as mass fraction of CeO ₂	Set Pd loading (wt %) in the total mass of the catalyst sample	Actual Pd loading (wt %) in the total mass of the catalyst sample
0.05	0.03	0.027
0.5	0.3	0.25
1	0.6	0.35
2	1.18	0.76
4	2.34	1.53

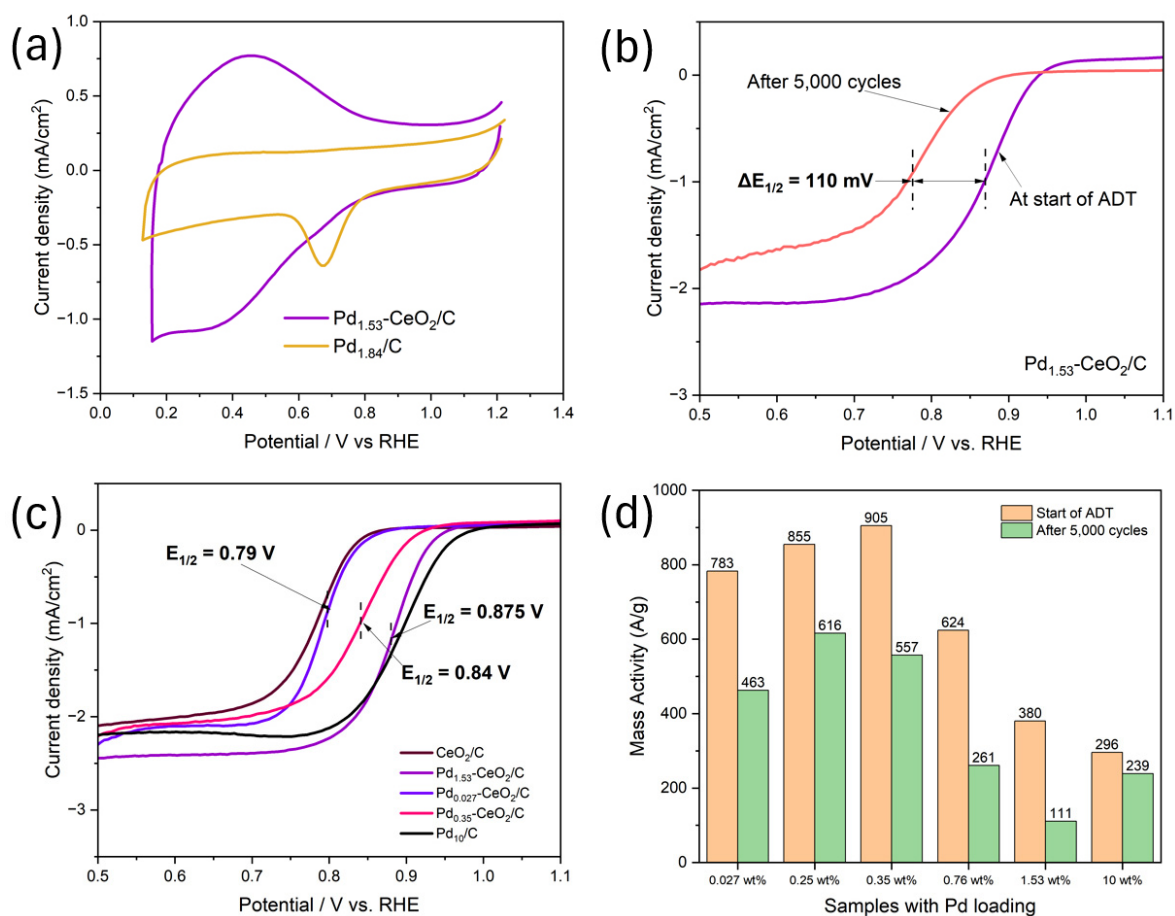


Figure S4. Electrochemical characterizations of Pd_x-CeO₂/C. (a), Cyclic voltammetry of Pd_{1.53}-CeO₂/C and Pd_{1.84}/C in N₂-saturated 1 M KOH solution at a scan rate of 50 mV/s and step size of 10 mV after 50 potential cycles; (b), ORR polarization curves of Pd_{1.53}-CeO₂/C measured at a rotation speed of 1,600 rpm in 1 M KOH solution at the beginning of ADT and after 5,000 potential cycles; (c), ORR polarization curves of pristine CeO₂/C, benchmark Pd₁₀/C, Pd_x/C, and some Pd_x-CeO₂/C samples measured at a rotation speed of 1,600 rpm in 1 M KOH solution, showing their $\Delta E_{1/2}$; and (d), calculated ORR mass activities of various Pd_x-CeO₂/C and benchmark Pd₁₀/C at the beginning of ADT and after 5,000 potential cycles.

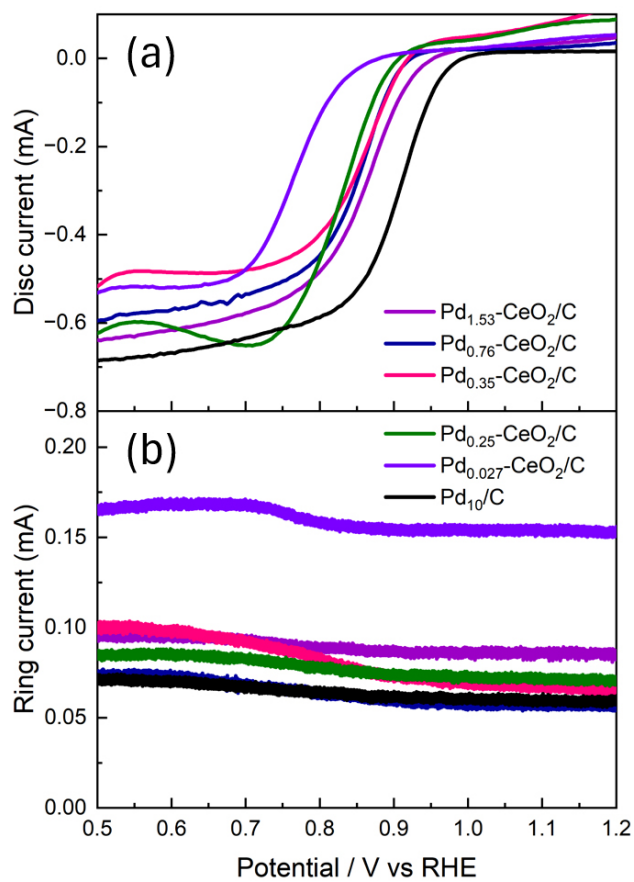


Figure S5. ORR polarization disc and ring currents of Pd_x-CeO₂/C and Pd₁₀/C determined in 1 M KOH at a rotation speed of 1,600 rpm using an RRDE system. (a), Disc current; (b) ring current.

Table S2: H₂O₂ production yield and molar rate estimated from the ring current by assuming a two-electron transfer pathway at a disc potential of 0.7 V vs. RHE

Catalysts	H ₂ O ₂ production yield		H ₂ O ₂ molar production rate	
	selectivity	<i>FE</i> *	(mol g _{Pd} ⁻¹ h ⁻¹)	(mol g _{catalyst} ⁻¹ h ⁻¹)
Pd _x -CeO ₂ /C				
<i>x</i> = 0.027	97.0%	94.2%	195.8	0.27
<i>x</i> = 0.25	51.0%	34.2%	100.8	0.14
<i>x</i> = 0.35	68.2%	51.7%	112.0	0.15
<i>x</i> = 0.76	50.7%	34.0%	82.1	0.11
<i>x</i> = 1.53	60.0%	42.8%	111.7	0.15
Pd ₁₀ /C	44.9%	28.9%	83.0	0.11

* *FE*: Faradaic efficiency.

Table S3: Comparison of H₂O₂ production performance across various metal-based electrocatalysts*

Catalyst	Structure or Size	Electrolyte	Mass activity	H ₂ O ₂ yield	Ref.
Ni-O-C nanosheets	atomic-level dispersion	1 M KOH	-	93% - 98% (selectivity) @ 0.3 - 0.9 V (RHE)	1
Al-O-C Ga-O-C Cr-O-C	atomic-level dispersion	0.1 M NaOH	23.9 (A/g-catalyst) 12.3 (A/g-catalyst) 6.1 (A/g-catalyst)	97% (selectivity) 89% (selectivity) 81% (selectivity) @ 0.7 V (RHE)	2
Pd-CNT Fe-CNT	atomic-level dispersion	0.1 M KOH	- 100 (A/g-catalyst) @ ~0.77 V (RHE)	~87% (selectivity) ~ 75 - 90% (selectivity) @ 0.4 - 0.75 V (RHE)	3
Co-POC-O	20 nm	0.1 M KOH	~12 (A/g-catalyst) @ 0.7 V (RHE)	~84% (selectivity) @ 0.7 V (RHE)	4
Co-N-C	> 50 nm	0.1 M KOH	-	~80% (selectivity) @ 0.1 V (RHE)	5
oxidized CNT	-	0.1 M KOH	~12.5 (A/g-catalyst) @ 0.7 V (RHE)	~90 % (selectivity) @ 0.4 - 0.7 V (RHE)	6
F-mrGO	> 1 μm	0.1 M KOH	100 (A/g-catalyst) @ 0.62 V (RHE)	~100% (selectivity) @ ~0.63 - 0.68 V (RHE)	7
Au-Pt-Ni NR	~50 nm	0.1 M KOH	31.7 (A/g-catalyst) 192.9 (A/g-Pt)	88 - 95% (selectivity) @ 0.1 - 0.6 V (RHE)	8
Pd/MnO ₂ -CNT Pd/CNT	atomic-level dispersion	0.1 M KOH	~484 A/g @ 0.9 V (RHE)	- ~25.3% (selectivity) @ 0.3 - 0.7 V (RHE)	9
In SAs/NSBC	atomic-level dispersion	0.1 M KOH	-	95.4% (selectivity) @ 0.66 V (RHE)	10
COF-366-Co	atomic-level dispersion	0.1 M KOH	-	91% (selectivity) @ 0.2 V (RHE)	11
Co ₁ @GO	chemical dispersion	0.1 M KOH	-	81.4 % (selectivity) @ 0.6 V (RHE)	12
Co-N-C	atomic-level dispersion	0.1 M KOH	~67 A/g @ 0.75 V (RHE)	~80% (selectivity) @ 0.6 V (RHE)	13
Co-F-CNT	atomic-level dispersion	1 M KOH	-	80% (selectivity) @ 0.2 – 0.8 V (RHE)	14
CoPc-OCNT	metal single-site on CNT	1 M KOH	-	96-98% (FE) @ 100 – 200 mA/cm ²	15
N-C	2D structure	1 M KOH	-	90% (FE) @ 0.55 – 0.65 V (RHE)	16
N-FLG-8	2D structure	1 M KOH	-	99% (FE) @ 1.8 V furfural oxidation in flow cell	17

Printex 6L C	--	1 M KOH		~60% (CE) @ -1.1 V (Ag/AgCl)	18
RuO _x /TNR	nanorods	1 M KOH in cathode		~90% (FE) @ 0.4 – 0.8 V (RHE)	19
Pd _{0.027} -CeO ₂ /C	clusters	1 M KOH	783 (A/g-Pd) @ 0.85 V (RHE)	97.0% (94.2%, FE) @ 0.7 V (RHE)	this work

* Co-POC-O: Co-N_x-C site and oxygen functional group co-modified carbon-based catalyst; F-mrGO: few-layered mildly reduced graphene oxide; CNT: carbon nanotube; NR: nano-rods; In SAs/NSBC: In atoms are anchored by combined N, S-dual first coordination and B second coordination supported by the hollow carbon rods; COF-366-Co: Co-centered conjugated porphyrin-based covalent organic framework coordination 2D polymer; Co₁@GO: Co single cobalt atoms anchored on oxygen functionalized graphene oxide; Co-F-CNT: Co single-atom sites with secondary fluorene heterodopants on carbon nanotubes; CoPc-OCNT: cobalt phthalocyanine molecule anchored on oxygen-modified carbon plane; FE: Faradaic efficiency; N-FLG-8: nitrogen-rich few-layered graphene (mass ratio between melamine and glycine: 8); N-C: modified nitrogen-doped carbon; RuO_x/TNR: ruthenium catalyst-decorated TiO₂ nanorods; Printex 6L C: unmodified Printex 6L carbon-based gas diffusion electrode (GDE); CE: current efficiency.

Table S4. Mass activity (MA) loss of Pd_x-CeO₂/C and Pd₁₀/C after 5,000 potential cycles

Catalyst	Loss of MA at $E_{1/2} = 0.85$ V
Pd _x -CeO ₂ /C	
$x = 0.027$	40.9%
$x = 0.25$	28.0%
$x = 0.35$	38.5%
$x = 0.76$	58.2%
$x = 1.53$	70.8%
Pd ₁₀ /C	19.3%

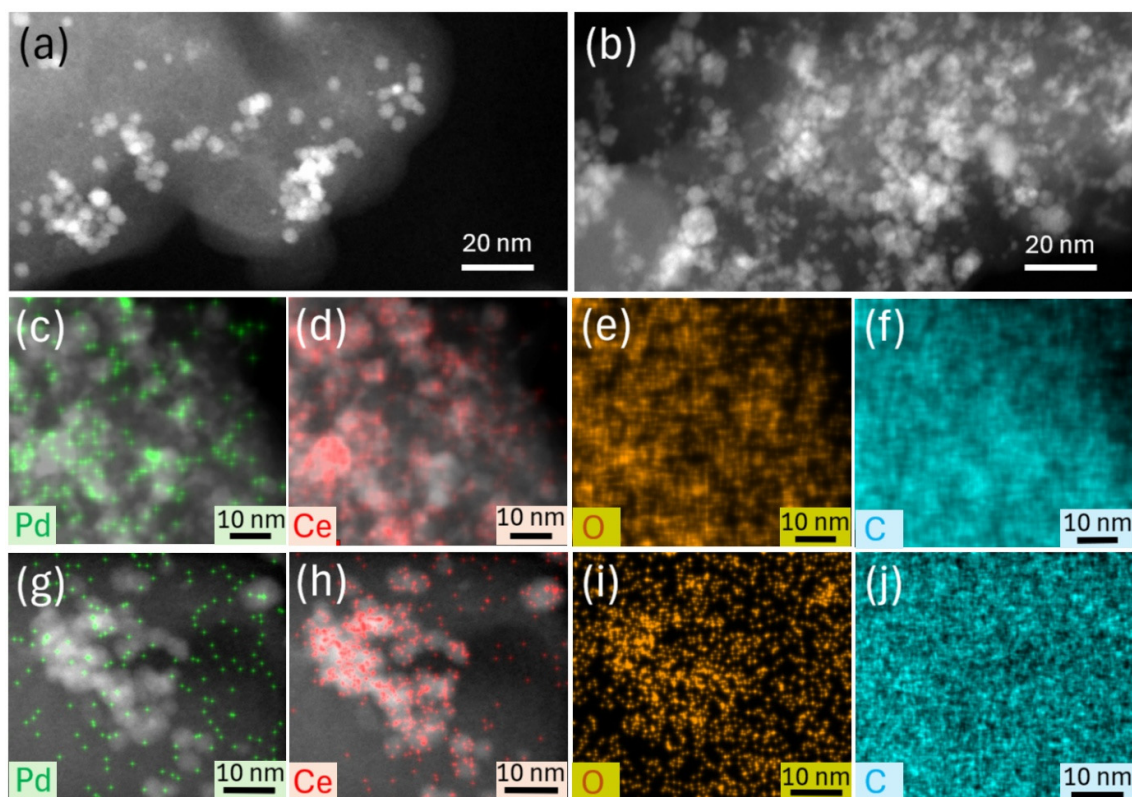


Figure S6. HAADF-STEM images and EDX elemental maps (Pd, Ce, O, and C) of Pd_{0.76}-CeO₂/C and Pd_{1.53}-CeO₂/C catalysts after 5,000-cycle ADT. (a) and (b), HAADF-STEM images of Pd_{0.76}-CeO₂/C and Pd_{1.53}-CeO₂/C after ADT, respectively; (c) – (f), EDX elemental maps of Pd_{1.53}-CeO₂/C; (g) – (j), EDX elemental maps of Pd_{0.76}-CeO₂/C. HAADF-STEM images are used as the background for Pd- and Ce-EDX maps.

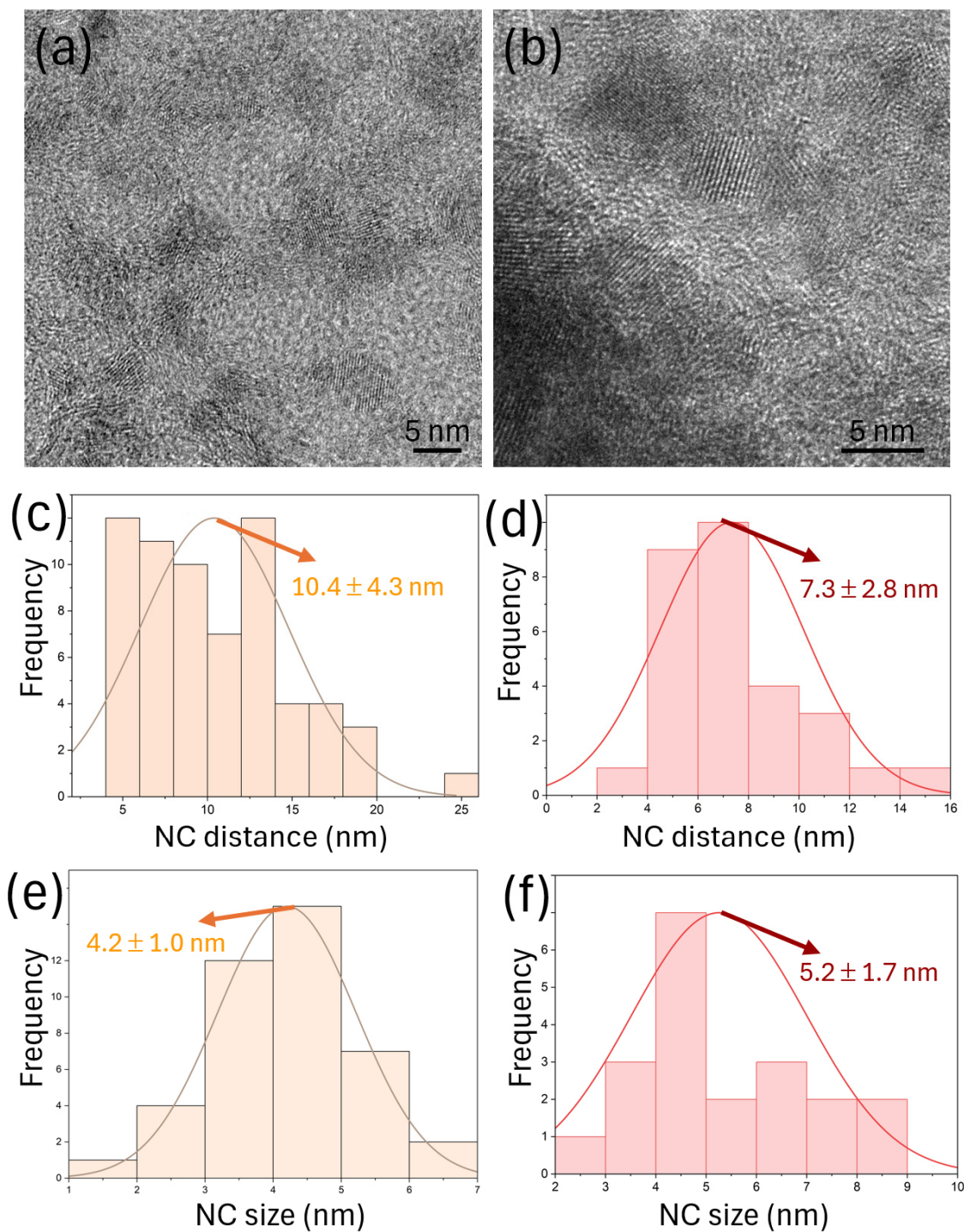


Figure S7. HRTEM images and corresponding data analysis of Pd_{1.53}-CeO₂/C before (a, c, e) and after ADT (b, d, f). (a) and (b), HRTEM images of the catalyst before and after 5,000-cycle ADT, respectively; (c) and (d), histograms of nearest-neighbor distances between PdO NCs; (e) and (f), size distribution of PdO NCs.

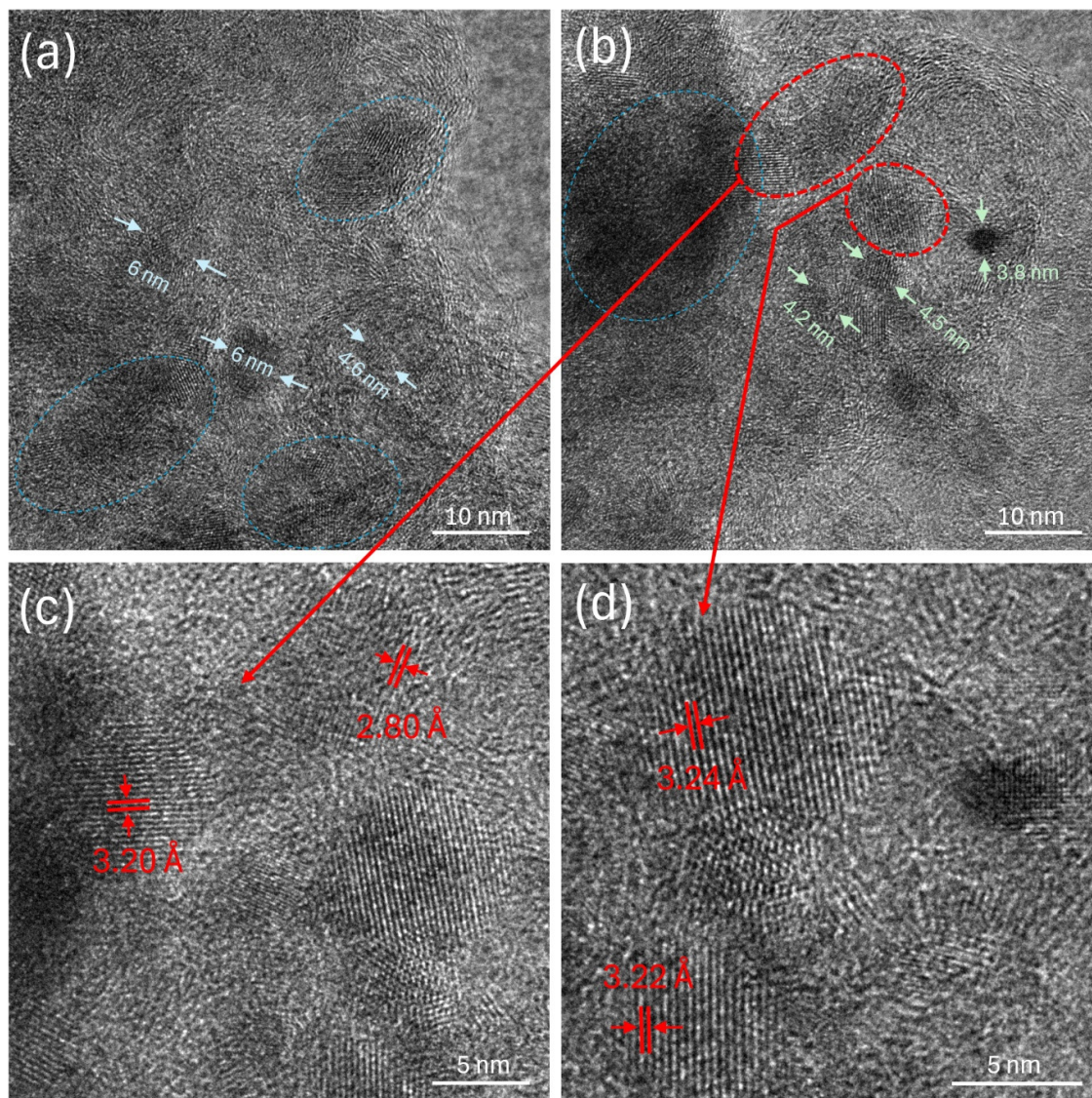


Figure S8. HRTEM images of Pd_{1.53}-CeO₂/C after 5,000-cycle ADT, taken from selected regions containing PdO NC agglomerations (highlighted with blue circles). (a) and (b), Size estimation of individual PdO NCs, illustrating that more severe agglomeration is associated with smaller surrounding satellite NCs; (c) and (d), magnified views of selected individual PdO NCs from panel (b), highlighted by red circles, showing the measured lattice spacings corresponding to specific crystallographic planes.

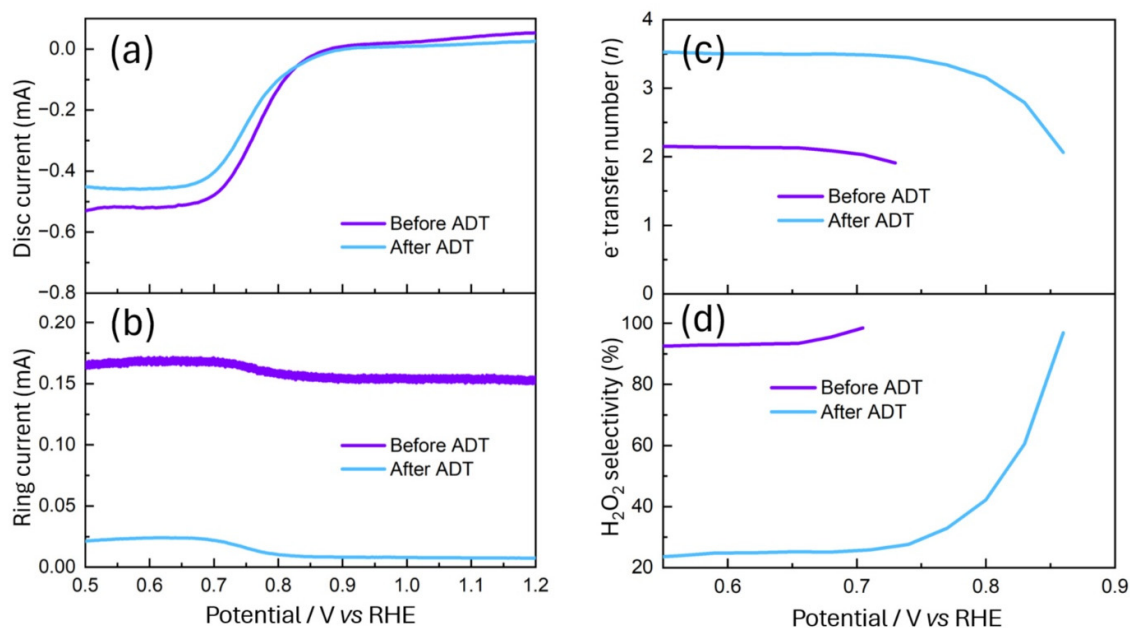


Figure S9. RRDE measurements of Pd_{0.027}-CeO₂/C before and after accelerated durability test (5,000 potential cycles) in 1 M KOH at a rotation speed of 1,600 rpm. (a) and (b), polarization disc current and ring current, respectively; (c) and (d), electron transfer numbers and H₂O₂ selectivity, respectively.

Table S5: Comparison of H₂O₂ yield on Pd_{0.027}-CeO₂/C before and after the accelerated durability test (5,000 potential cycles) conducted in 1 M KOH at a rotation speed of 1,600 rpm.

	Initial		After ADT	
	0.6 V	0.7 V	0.6 V	0.7 V
potential (RHE)	0.6 V	0.7 V	0.6 V	0.7 V
Selectivity	93.2%	97.0%	23.9%	25.8%
<i>FE</i> *	87.3%	94.2%	13.6%	14.8%
H ₂ O ₂ molar production rate (mol g _{Pd} ⁻¹ h ⁻¹)	205.6	195.8	43.9	39.5
(mol g _{catalyst} ⁻¹ h ⁻¹)	0.28	0.27	0.04	0.04

* *FE*: Faradaic efficiency.

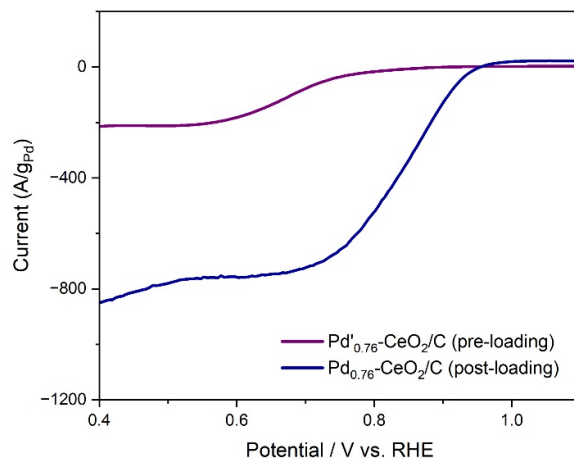


Figure S10. Comparison of ORR polarization curves of sample Pd_{0.76}-CeO₂/C and Pd'_{0.76}-CeO₂/C generated from the “pre-loading” method.

References:

1. W. Xu, Z. Liang, S. Gong, B. Zhang, H. Wang, L. Su, X. Chen, N. Han, Z. Tian, T. Kallio, L. Chen, Z. Lu and X. Sun, *ACS Sustainable Chem. Eng.*, 2021, **9**, 7120-7129.
2. Q. Yang, W. Xu, S. Gong, G. Zheng, Z. Tian, Y. Wen, L. Peng, L. Zhang, Z. Lu and L. Chen, *Nat. Commun.*, 2020, **11**, 5478.
3. K. Jiang, S. Back, A. J. Akey, C. Xia, Y. Hu, W. Liang, D. Schaak, E. Stavitski, J. K. Nørskov, S. Siahrostami and H. Wang, *Nat. Commun.*, 2019, **10**, 3997.
4. B.-Q. Li, C.-X. Zhao, J.-N. Liu and Q. Zhang, *Adv. Mater.*, 2019, **31**, 1808173.
5. Y. Sun, L. Silvioli, N. R. Sahraie, W. Ju, J. Li, A. Zitolo, S. Li, A. Bagger, L. Arnarson, X. Wang, T. Moeller, D. Bernsmeier, J. Rossmeisl, F. Jaouen and P. Strasser, *J. Am. Chem. Soc.*, 2019, **141**, 12372-12381.
6. Z. Lu, G. Chen, S. Siahrostami, Z. Chen, K. Liu, J. Xie, L. Liao, T. Wu, D. Lin, Y. Liu, T. F. Jaramillo, J. K. Nørskov and Y. Cui, *Nat. Catal.*, 2018, **1**, 156-162.
7. H. W. Kim, M. B. Ross, N. Kornienko, L. Zhang, J. Guo, P. Yang and B. D. McCloskey, *Nat. Catal.*, 2018, **1**, 282-290.
8. Z. Zheng, Y. H. Ng, D.-W. Wang and R. Amal, *Adv. Mater.*, 2016, **28**, 9949-9955.
9. W. Xiang, Y. Zhao, Z. Jiang, X. Li, H. Zhang, Y. Sun, Z. Ning, F. Du, P. Gao, J. Qian, K. Kato, M. Yamauchi and Y. Sun, *J. Mater. Chem. A*, 2018, **6**, 23366-23377.
10. E. Zhang, L. Tao, J. An, J. Zhang, L. Meng, X. Zheng, Y. Wang, N. Li, S. Du, J. Zhang, D. Wang and Y. Li, *Angew. Chem. Int. Ed.*, 2022, **61**, e202117347.
11. C. Liu, H. Li, F. Liu, J. Chen, Z. Yu, Z. Yuan, C. Wang, H. Zheng, G. Henkelman, L. Wei and Y. Chen, *J. Am. Chem. Soc.*, 2020, **142**, 21861-21871.

12. B.-W. Zhang, T. Zheng, Y.-X. Wang, Y. Du, S.-Q. Chu, Z. Xia, R. Amal, S.-X. Dou and L. Dai, *Commun. Chem.*, 2022, **5**, 43.
13. E. Jung, H. Shin, B.-H. Lee, V. Efremov, S. Lee, H. S. Lee, J. Kim, W. Hooch Antink, S. Park, K.-S. Lee, S.-P. Cho, J. S. Yoo, Y.-E. Sung and T. Hyeon, *Nat. Mater.*, 2020, **19**, 436-442.
14. Y. Tian, R. Chen, X. Liu, L. Yin, D. a. Yang, F. Hou and J. Liang, *EcoMat*, 2023, **5**, e12336.
15. P. Cao, X. Quan, X. Nie, K. Zhao, Y. Liu, S. Chen, H. Yu and J. G. Chen, *Nat. Commun.*, 2023, **14**, 172.
16. B. Sabri Rawah, M. Albloushi and W. Li, *Chem. Eng. J.*, 2023, **466**, 143282.
17. L. Li, C. Tang, Y. Zheng, B. Xia, X. Zhou, H. Xu and S.-Z. Qiao, *Adv. Energy Mater.*, 2020, **10**, 2000789.
18. W. R. P. Barros, T. Ereno, A. C. Tavares and M. R. V. Lanza, *ChemElectroChem*, 2015, **2**, 714-719.
19. T. H. Jeon, B. Kim, C. Kim, C. Xia, H. Wang, P. J. J. Alvarez and W. Choi, *Energy Environ. Sci.*, 2021, **14**, 3110-3119.